EUROPEAN ORGANIZATION FOR NUCLEAR RESEARCH

CERN/EP 82-150
1 October 1982

PROTONIUM SPECTROSCOPY AND IDENTIFICATION OF P-WAVE AND S-WAVE INITIAL STATES OF $p\bar{p}$ ANNIHILATIONS AT REST WITH THE ASTERIX EXPERIMENT AT LEAR

The ASTERIX* Collaboration

S. Ahmad[4], C. Amsler[6], R. Armenteros[1], E. Auld[5], D. Axen[5], G. Beer[5], J.C. Bizot[4], M. Caria[6], M. Comyn[5], W. Dahme[3], B. Delcourt[4], K. Erdman[5], P. Eschtruth[4], U. Gastaldi[2], M. Heel[2], R. Howard[5], J. Jeanjean[4], H. Kalinowsky[2], F. Kayser[2], E. Klempt[2], R. Landua[2], H. Nguyen[4], L. Robertson[5], C. Sabev[1], R. Schneider[2], O. Schreiber[2], U. Straumann[6], P. Truöl[6], B. White[5] and W.R. Wodrich[3]

(Presented by U. Gastaldi)

INTRODUCTION

The ASTERIX experiment has been designed[1] with three main objectives:

(a) To study the general features of $p\bar{p}$ interactions at rest: strong interaction shift and broadening of the atomic levels of the $p\bar{p}$ atom, branching ratios of the $p\bar{p}$ annihilation channels from S and P atomic states, spin dependence of shifts, widths and branching ratios;

(b) To extend (with comparable resolution, better reconstruction of final states, about 100 times more statistics and data both with P-wave and S-wave initial states) the work done so far in the spectroscopy of light mesons produced in $p\bar{p}$ annihilations at rest[2];

Invited paper at the Workshop on Physics at LEAR With Low Energy Cooled Antiprotons 9-16 May 1982, Erice, Sicily

---

* Antiproton STop Experiment with tRigger on Initial X-rays. CERN[1], Mainz[2], Munich[3], Orsay[4] (LAL), Vancouver-Victoria-TRIUMF[5], Zürich[6].

(c) To search with high sensitivity for gluonium (gg, ggg bound states), $qq\bar{q}\bar{q}$ baryonium structures and NN states bound by strong interactions. These objects are likely to be produced in $p\bar{p}$ annihilations at rest besides the well-known $q\bar{q}$ light mesonic structures already seen in bubble chamber experiments.

The detection system has a large acceptance, provides for every event simultaneous information on both the initial atomic state and the final annihilation products and can be triggered on preselected initial and/or final state configurations. Figs 1 and 2 illustrate the experimental apparatus. Antiprotons coming along the axis of a solenoidal magnetic spectrometer, cross a moderator and a thin scintillator and are stopped in a H_2 gas target at normal pressure. The H_2 target is surrounded by a projection chamber capable of detecting the X-ray atomic transitions to the 1S, 2P and 3D atomic levels of protonium. The chamber identifies X-rays and measures their energy and the three co-ordinates of their absorption point. The charged particles emitted in each $p\bar{p}$ annihilation are imaged by the projection chamber and their momentum is measured by the cylindrical MWPC's that equip the spectrometer (acceptance > 50%). Planar MWPC's at each end cap increase the solid angle for detecting prongs. Gamma detection with determination of the γ conversion point is ensured over nearly the entire solid angle by lead converter foils inserted between the planar chambers in the end caps and before the two outermost cylindrical chambers (the γ conversion probability is typically 30%).

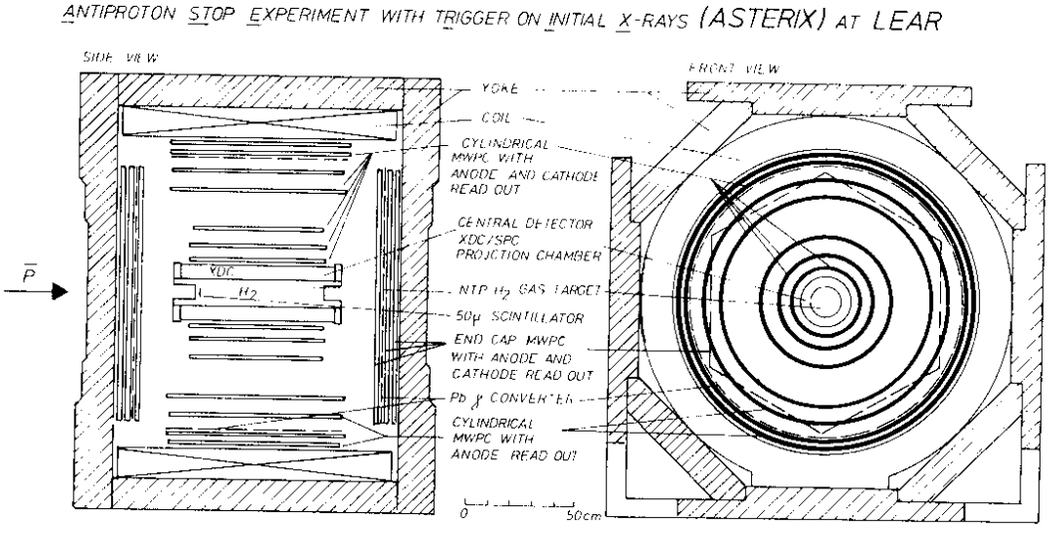

Fig. 1. Schematic views of the experimental apparatus.

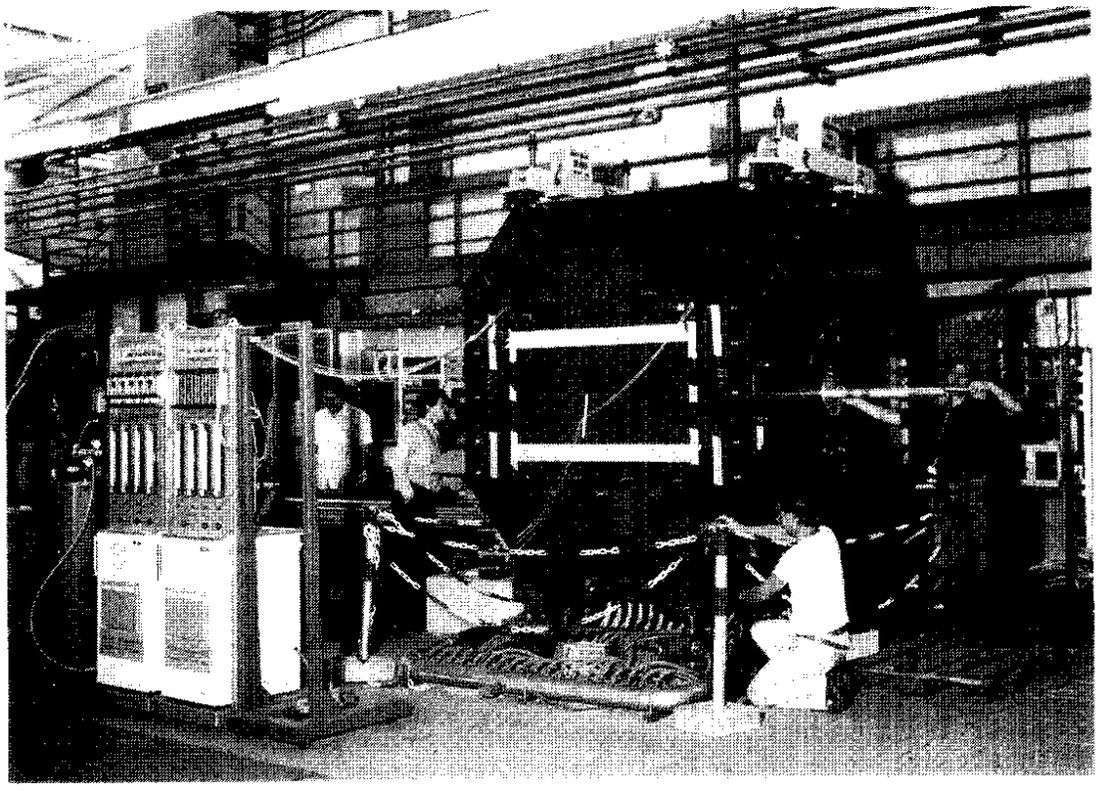

Fig. 2. The ASTERIX version of the DM1 solenoidal spectrometer[3] in the CERN PS South Hall, after shipment from LAL Orsay, during magnetic field measurements in July 1982.

Besides the new high event rate common to all LEAR experiments the distinctive features of the ASTERIX experiment are:

(a) The use of a gaseous H_2 target instead of a conventional liquid H_2 one. This way the probability that X-ray transitions to the 3D, 2P and 1S levels of protonium occur and can be detected is largely increased, and an important fraction of annihilations at rest occur from P levels of the $p\bar{p}$ atom.

(b) An X-ray detector of large overall detection efficiency, low energy threshold and low background rate that permits to identify individually P-wave and S-wave annihilation events from 2P and 1S levels of protonium and has an adequate energy resolution to observe the effects of strong interactions on the 1S levels of protonium.

(c) A detection system for the products of $p\bar{p}$ annihilations that permits to fully reconstruct final states with several prongs and up to one neutral pion; resonant states produced in annihilation channels that can be fully reconstructed can be observed and studied in detail.

(d) A trigger system that permits to filter the acquisition of events by means of two independent chains of processors working in parallel. One chain can select initial states of $p\bar{p}$ annihilations on the basis of the information provided by the X-ray detector; the second chain can select final states by exploiting information from the central detector, the magnetic spectrometer and the γ detector (prongs and γ multiplicities, momentum of charged particles).

The first two sections of this paper focus on the impact on our experimental program of the choice of a gas target and of a large acceptance X-ray detector. These choices should permit us to get basic information in protonium spectroscopy and will bring in the new possibility of studying P-wave annihilations and of comparing P-wave and S-wave annihilations. In the second half of the paper we discuss the rate and the signature of antiprotons stopping in the gas target, we describe the X-ray detector and results from some initial tests and give estimates of the performances of the apparatus expected for protonium spectroscopy and identification of initial states. The detection system for the reconstruction of final states of $p\bar{p}$ annihilations and its sensitivity to identify resonances in various annihilation channels are covered in the paper presented by W. Dahme[4], where also the general motivations for studying the spectroscopy of light mesons and searching for exotic resonances are discussed. A comprehensive description of the apparatus is given in the proposal of our experiment[1], together with an overview of the status of $p\bar{p}$ experiments at rest.

PROTONIUM CASCADE AND SPECTROSCOPY

Fig. 3 shows X-ray transitions of the K, L and M series that can be detected. These transitions provide information on the cascade of the $p\bar{p}$ atom and can be used to determine the shift ΔE and broadening Γ of protonium levels caused by strong interactions.

ΔE_{1S} and $\Gamma_{1S}/2$ are expected to be of the order of $0.5 \div 1$ KeV[5]. These quantities are directly related to the zero energy $p\bar{p}$ S-wave scattering length and are sensitive to the presence of hadronic bound states of $p\bar{p}$ and to $p\bar{p}$ resonances near to the $2\,m_p$ mass threshold. No direct measurement of these quantities is available, because at present no clear K X-ray line has been detected.

In order that X-ray transitions to the lower levels of the $p\bar{p}$ atom occur it is of course necessary that the atomic cascade does not stop before these transitions can take place. In high pressure and liquid H_2 targets the collisional Stark mixing effect rapidly populates S levels with high principal quantum

number n. S levels decay dominantly via annihilation and consequently the population of all low n levels is drastically reduced. In H_2 gas the situation is more favourable. One experiment made in 1977 at CERN with participation of part of our collaboration has shown that the 2P level is reached with a probability $Y_{2P} \approx 5\%$ in a H_2 gas target at 4 atm pressure[6].

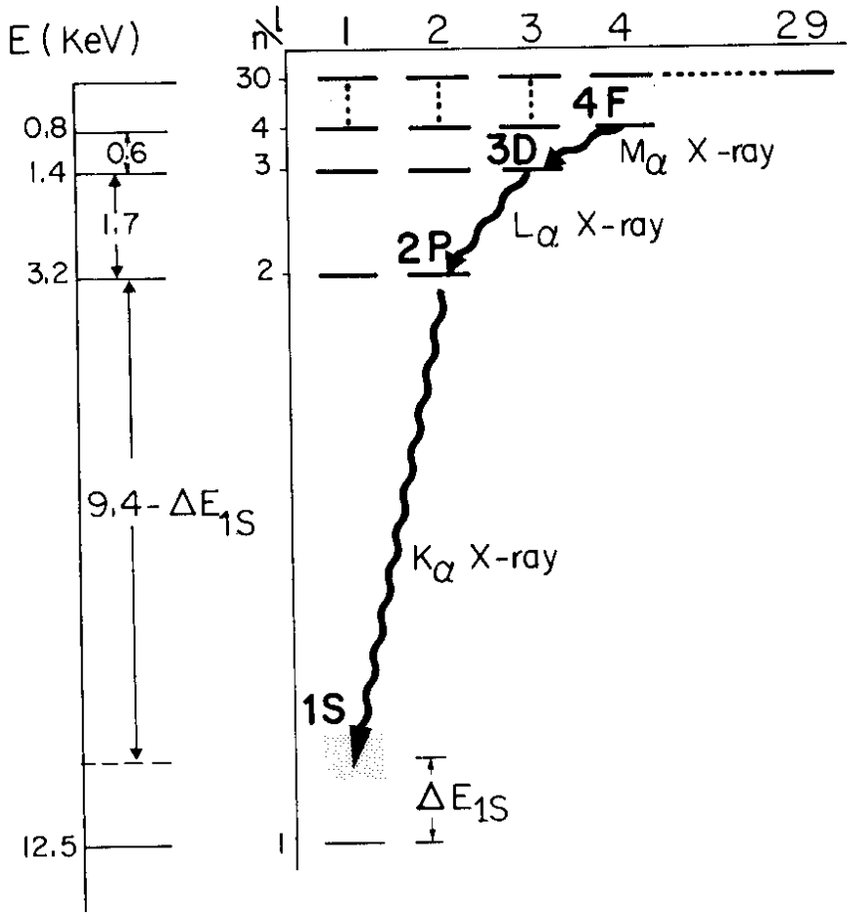

Fig. 3. Levels of the $p\bar{p}$ atom and some detectable X-ray transitions

Y_{2P} can be made larger by reducing the target pressure. By having the $p\bar{p}$ atom in vacuum Y_{2P} could increase up to nearly 100%[7]. We have chosen to work at atmospheric pressure where one could expect $Y_{2P} \sim 10\%$ and where a vacuum vessel can be avoided which would spoil the missing momentum resolution of the charged particle spectrometer.

A gas target can be surrounded by a gas proportional chamber with target and counter gas separated by a thin mylar window[8]. We have constructed a new detector which is used as X-ray drift chamber[9] for pp X-rays and as a spiral projection chamber[10] to image the pp annihilation prongs close to the target. The overall

X-ray detection efficiency is larger than 50% in the energy range from 2 to 10 KeV and the energy resolution for X-rays is about 20% FWHM at 5.9 KeV. This allows a clean separation between L and K lines and will permit to use XDC X-ray signals as a flag and later on as a trigger for P- and S-wave annihilation events. This relatively modest energy resolution is also sufficient for a measurement of the energy of the K X-rays, whose natural line width is expected to be about 1 KeV. The total annihilation width of the 2P level Γ_{2P} - which is expected to be of the order of 0.04 eV - can be determined by counting how many K_α X-rays are emitted for a given number of detected L X-rays. For this measurement a high detection efficiency and a low level of background are essential as the radiative width of the 2P level is only 0.00037 eV.

The spin triplet and spin singlet ground states of protonium are expected to show different energy shifts and broadenings[5]. In many calculations the difference in shifts is of the order of only 200 eV for two lines with expected widths of 1000 eV. This would make it hard to determine ΔE and Γ separately for the levels 1^1S_0 and 1^3S_1, since the observable X-ray spectrum would be just a slightly asymmetric line. We plan to separate X-ray transitions to the singlet and triplet ground state by selecting with the magnetic spectrometer final states of S-wave annihilation that can come unambiguously either from the singlet or the triplet state (fig. 4).

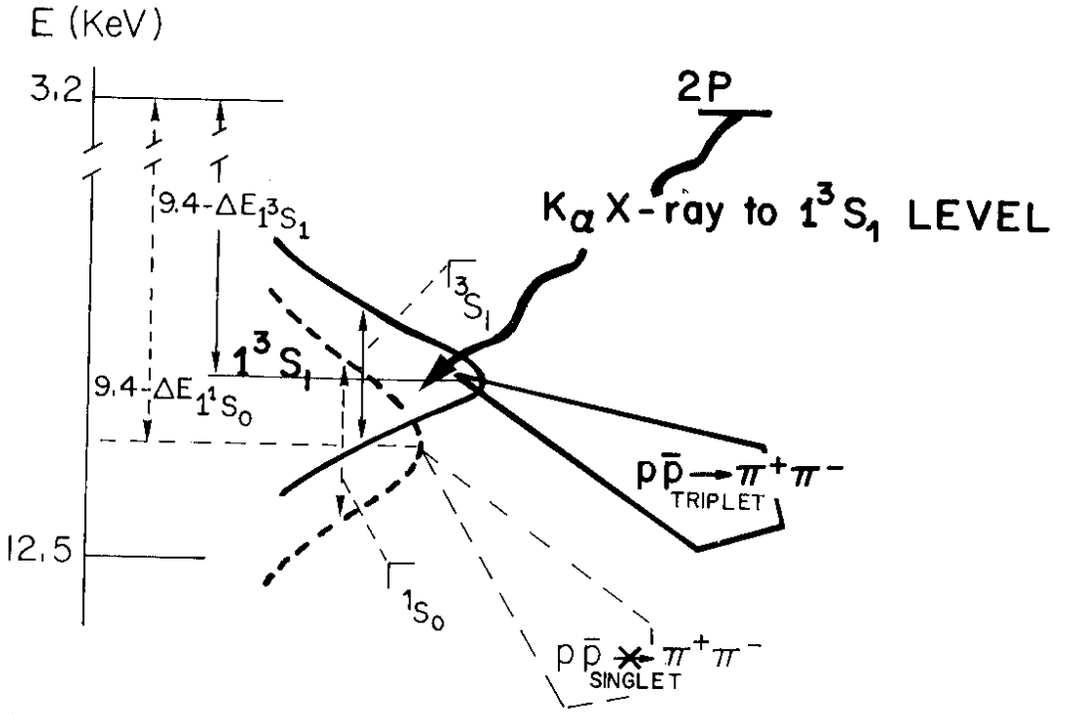

Fig. 4. Use of information on the final state of $\bar{p}p$ annihilations to single out the triplet ground state line and measure its shift $\Delta E_{^3S_1}$, and broadening $\Gamma_{^3S_1}$.

COMPARISON OF S-WAVE AND P-WAVE $p\bar{p}$ ANNIHILATIONS AT REST

In liquid H_2 targets $p\bar{p}$ annihilations at rest occur dominantly from high n S states, according to the results of bubble chamber experiments, that provide the majority of existing data on branching ratios of annihilation channels. The only evidence of P-wave annihilation in liquid H_2 comes in the rare two pion annihilation channel from the observation of $\pi^0\pi^0$ events[11].

Quite differently P-wave annihilation is frequent in a H_2 gas target, with which it therefore becomes possible to compare S- and P-wave annihilations. The experiment of the Protonium Collaboration mentioned above[6] has shown that the atomic 2P level, once populated by radiative transitions, annihilates in more than 90% of the cases, while it radiates K_α X-rays in less than 10% of the cases. The experimental evidence for this fact is displayed in fig. 5. L X-rays populating the 2P level were clearly seen above a smooth and low background, while there is no evidence for a K_α X-ray peak, which should have been observed (shaded area) if annihilation from the 2P level would be negligible (see ref. 6 for a more detailed discussion). Since also 3P, 4P ... and higher n P levels are populated by the atomic cascade and the population of the 2P level alone is already 5%, the fraction of P-wave annihilation at 4 atm. pressure is larger than 5%. Cascade calculations (whose predictive power is limited as the strong interaction shifts and widths of the atomic levels are not known) suggest that annihilation in P- and S-wave may be equally frequent at 1 atm[12].

By recording $p\bar{p}$ annihilation events in a H_2 gas target the data will contain a large fraction of P-wave annihilation from the various nP-levels from which it can occur. Without direct information on the initial state it is in general not possible to separate S-wave annihilation events from P-wave annihilation events. It is possible to increase the content of P-wave annihilation by reducing the pressure but the exact percentage depends on the atomic cascade and a detailed experimental study of it will be necessary before knowing exactly the ratio between S-wave and P-wave annihilation. We plan therefore to select events with P-wave annihilation by requiring a L X-ray transition detected in coincidence. If the background in the L X-ray region is negligible, this set of P-wave annihilation events will be contaminated only by those events in which a K_α X-ray was emitted and escaped detection.

Events where a K_α X-ray was detected will be much more rare, but will provide a pure sample of S-wave annihilations, as a K X-ray identifies unambiguously a 1S atomic level. Moreover if it should turn out that the physical separation between triplet

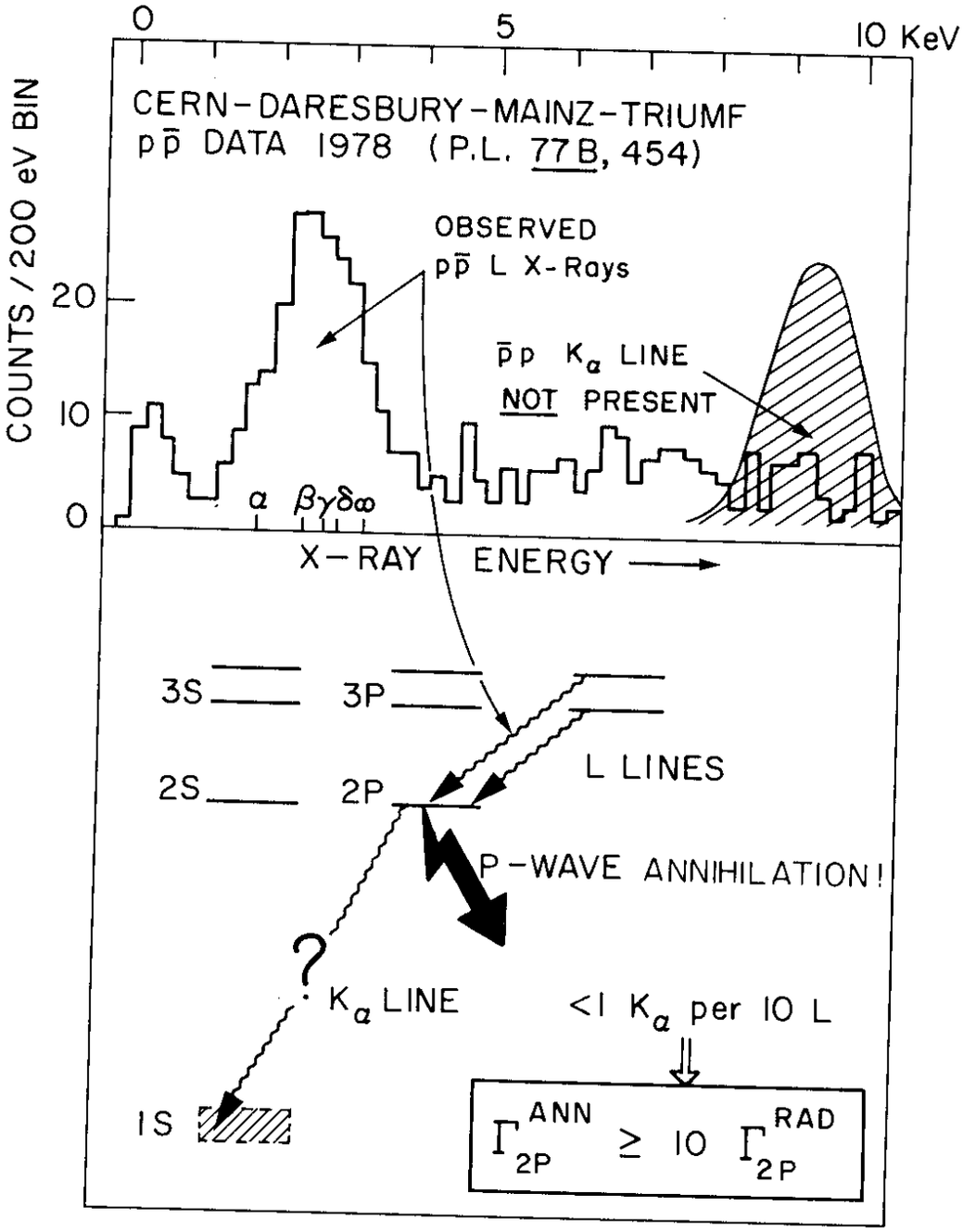

Fig. 5. P-wave annihilation from 2P levels of protonium.

and singlet ground states is appreciable, then it would become possible to use the information of the K_α X-ray energy to select singlet and triplet annihilation events as illustrated in fig. 6. Notice that the modest energy resolution of our detector

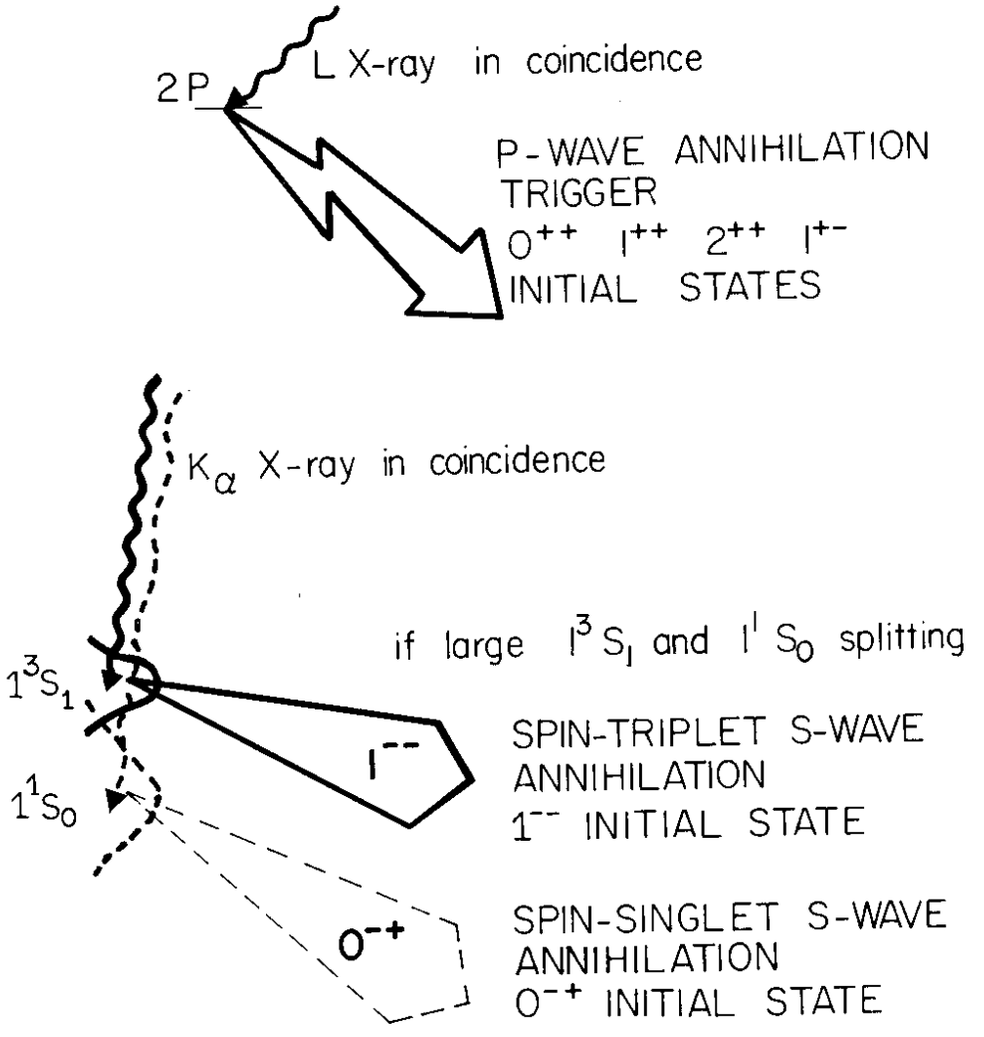

Fig. 6. Use of X-ray information to separate annihilation reactions from initial states with different quantum numbers.

would not rule out this possibility if the singlet and triplet line are well separated, as a differential absorber foil could be used in front of the X-ray detector to suppress the more energetic line. All this appears very interesting because of the possibilities connected to a comparison of S-wave annihilation data in different $p\bar{p}$ spin states. However, as mentioned previously, so far not even a clear K X-ray signal has been detected, and it is not at all sure that we will be able to distinguish X-rays going to the singlet state from X-rays going to the triplet states.

We plan to collect data on P-wave and S-wave annihilations with high statistics (typically 10^7 analysed events instead of 10^5 events which were analysed in bubble chamber experiments). The comparison of the two sets of data is likely to give substantial information on the dynamics of $p\bar{p}$ interactions and could help in identifying glueball candidates. Moreover, P-wave annihilations may be indispensable for producing narrow baryonium states. Let us briefly elaborate on these points.

At rest the phase space available for a given $p\bar{p}$ annihilation final state is the same within 10 KeV for annihilations from S- and P-wave atomic states. Therefore, differences that may show up when comparing branching ratios and the shape of invariant mass spectra will immediately indicate different dynamics in annihilation processes occuring in S and P-waves. At present the dynamics of $p\bar{p}$ annihilations is not understood at all. In boson exchange models of $p\bar{p}$ interactions used to predict baryonium states, the annihilation is described by an imaginary potential not dependent on the quantum numbers of the $p\bar{p}$ state. Our experiment will determine for several final states the relative branching ratios both for P-wave initial states and S-wave initial states. The observation of a dependence on the initial state of the annihilation branching ratios into a given final or intermediate state would be the first experimental proof that the annihilation potential does depend on quantum numbers and that the annihilation is not "black". If this is the case any comprehensive model of $p\bar{p}$ interactions at low energies should also predict S- and P-wave branching ratios for annihilations at rest.

One of the main motivations for LEAR has been the possibility of discovering and studying in detail the spectroscopy of $qq\bar{q}\bar{q}$ baryonium states and $N\bar{N}$ strongly bound states. These objects could be quite broad due to the large annihilation probability and hence difficult to observe experimentally. Those with high angular momentum might be narrower because of the protective centrifugal barrier and then easier to identify. Transitions from atomic $p\bar{p}$ states to baryonium states are expected to change the initial angular momentum by one unit typically[13]. Hence the interest of starting from P levels to reach D states. This could really give a chance to find narrow baryonium, which was looked for so far only in liquid targets, where its production mechanism could be largely suppressed for the reasons mentioned before. Notice that at LEAR, while all experiments looking for $p\bar{p}$ X-ray lines will use gas targets, only the ASTERIX experiment has adopted a gas target to search for baryonium starting also from P states. Other experiments at rest focusing on baryonium have been planned with liquid targets (thus limiting themselves mainly to annihilations in S-wave initial states).

A fundamental discovery possible at LEAR is that of gg and ggg gluonium states[14]. Glueballs are required to exist by quantum chromodynamics and the proof of their existence would test the fundamental assumption of the theory that gluons - the mediators of the strong interaction between quarks - interact among themselves. The best existing glueball candidate was observed in radiative ψ decays[15]. This state was first seen as early as 1963 in $p\bar{p}$ annihilations at rest in the 80 cm H_2 bubble chamber at CERN[16,17]. The pp annihilation data provide a clear peak (see fig. 7 from ref. 17) which contains 5 times more events

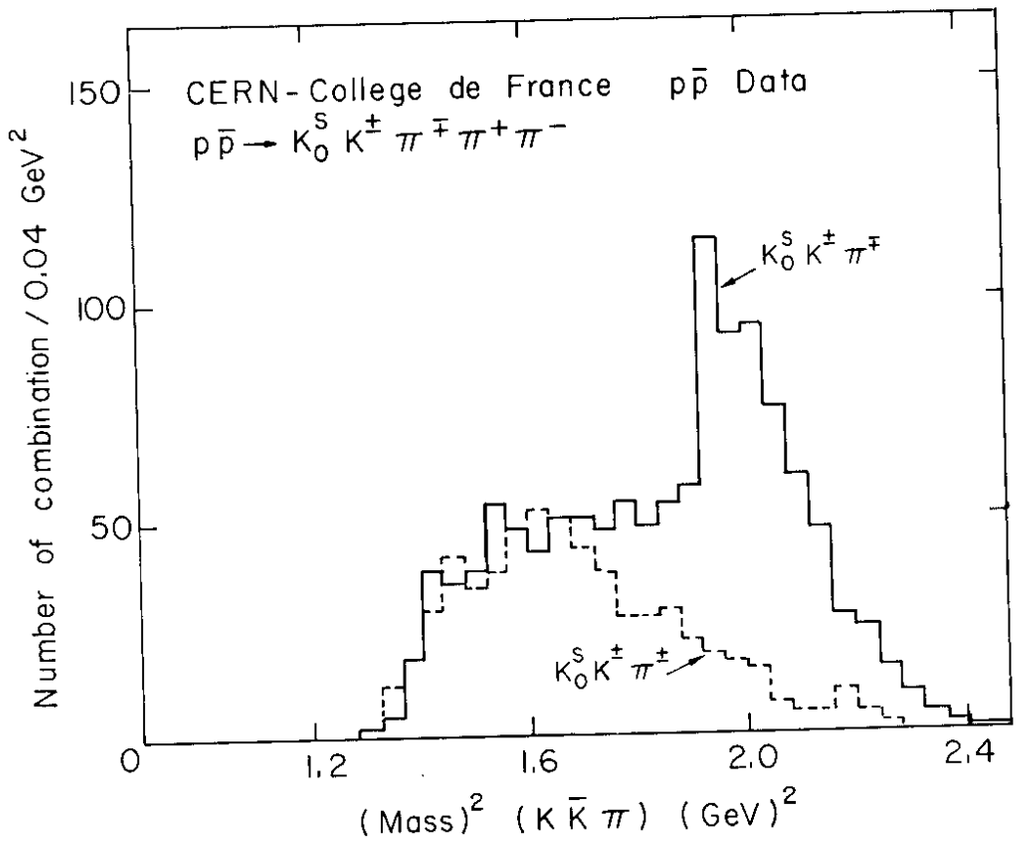

Fig. 7. Glueball candidate decaying into $K^{S}_{0}K^{\pm}\pi^{\mp}$ in $p\bar{p}$ annihilations at rest.

than the peaks observed in radiative ψ decays. In our experiment we will increase the statistics by at least a factor of 10. This peak was quite likely produced in S-wave $p\bar{p}$ annihilations as the data were taken with a liquid H_2 bubble chamber. The point of interest here is: how would the spectra of fig. 7 look like for P-wave annihilations? In $p\bar{p}$ P-wave annihilations the initial states have quantum numbers 0^{++}, 1^{++}, 2^{++} and 1^{+-}, while in $p\bar{p}$ S-wave annihilation the initial states have quantum numbers 0^{-+} and 1^{--}.

In our experiment we should be able to get separately invariant mass spectra for P-wave and S-wave $\bar{p}p$ annihilations leading to final states composed of the same particles. Should the mass spectrum of a particular combination of particles indicate the presence of a resonance either in only one or in both final states, its quantum numbers could be, if not fixed uniquely, at least reduced to a very much limited set of possibilities. Comparison of the two spectra could also give hints about the presence of broad resonances and hence motivate a more detailed analysis.

$\bar{p}$ STOP AND FORMATION OF $p\bar{p}$ ATOMS

Our H_2 gas target has a useful length of $\sim$ 60 cm (fig. 8). One has to compare this length with the width of the range curve of antiprotons in H_2 gas to get the fraction of antiprotons in the beam that stop in the target and form $p\bar{p}$ atoms. In table 1 we indicate the number of antiprotons in the beam necessary to stop 100 $\bar{p}$'s in the target. For an incoming $\bar{p}$ beam with momenta below 200 MeV/c all antiprotons entering the H_2 target will be stopped.

Table 1. Number of $\bar{p}$ necessary to form 100 $p\bar{p}$ atoms in the ASTERIX target.

$\bar{p}$ in beam	P_{Lab} MeV/c)	$\bar{p}$ range in C ($g\ cm^{-2}$)	Length of $\bar{p}$ STOP volume (cm H_2 at 1 atm)	$\bar{p}$ STOP in ASTERIX H_2 target
6000	600	23.	$\sim$ 3600	100
600	300	2.3	$\sim$ 360	100
100	100	0.04	$\sim$ 8	100
100	20	$\gtrsim 10^{-4}$	$\lesssim$ 0.1	100

By lowering the beam momentum the length of the stop volume reduces and, if it is possible to go down to 20 MeV/c, all antiprotons will stop inside a volume of the order of 1 mm^3. At low beam momenta a very thin target entrance window is necessary to let the antiprotons enter the H_2 gas. We have less than 100 μm of material mounted permanently between the end of the vacuum beam pipe and the H_2 target, so we can accept beams from LEAR with momenta lower than 100 MeV/c. At higher beam momenta we will have a moderator before the target window. The moderator will be the plastic scintillator disk T1 (viewed by an air light guide). At the entrance of the H_2 target there is a 50 μm thick plastic scintillator located between two aluminized mylar reflectors and viewed by a tube of lucite light guide (T2 in fig. 8). T2 is surrounded by a tube of scintillator material (T3) (fig. 9).

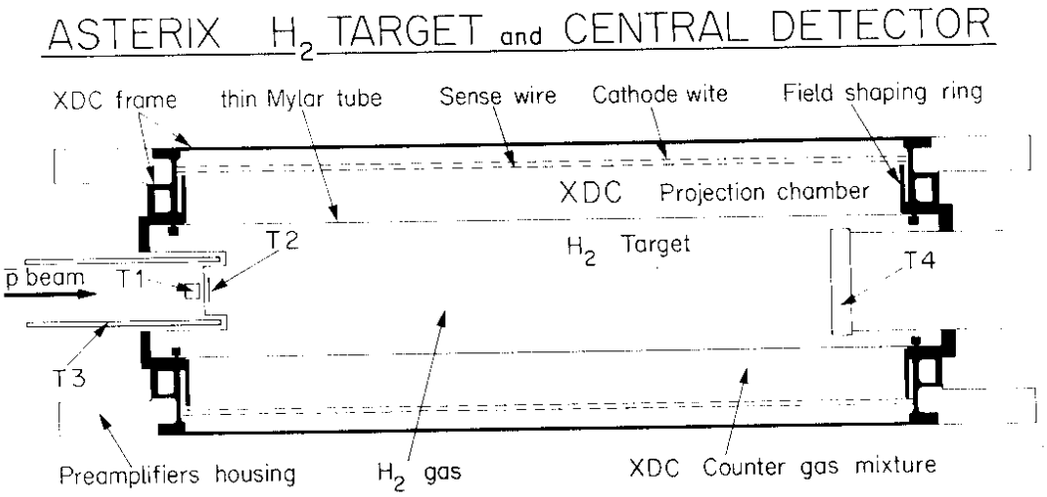

Fig. 8. H_2 target (16 cm diameter), XDC central detector and T1, T2, T3 and T4 plastic scintillators.

At the other extreme of the target a 2 cm thick scintillator disk (T4) is positioned. By adjusting the thickness of the moderator one can set the maximum of the $\bar{p}$ range curve in the centre of the target. A fraction of $\bar{p}$'s stops in the moderator and in T2, a fraction in H_2 and a fraction in T4. We use the signal (T2, $\overline{T3}$, $\overline{T4}$) as fast p STOP trigger. This signal is also used as START signal for drift time measurements. Antiprotons stopping in T2 ($\sim$ 5 mg cm^{-2}) can simulate $\bar{p}$'s stopping in the H_2 gas. T3 vetoes most of the antiprotons stopped in T2 since it has a high probability of detecting at least one prong from $\bar{p}$ annihilations in T2 or nearby.

Fig. 9. Assembly of the T2 and T3 scintillators and light guides. Light sent from a lamp into one arm of the T2 light guide diffuses out from the lucite dome supporting the 50 µm thick T2 scintillator.

Notice that we can get a usable light output from T2 because $\bar{p}$'s at the end of the range ionize two orders of magnitude more than when they are minimum ionizing. We have chosen a diameter of 16 cm for the target as a compromise so as not to have too many $\bar{p}$'s scattering out of the target into the central detector XDC at momenta $\gtrsim$ 300 MeV/c. When LEAR works reliably below 200 MeV/c it will be possible to reduce the diameter of our target and to increase correspondingly the active volume of the central detector. At low $\bar{p}$ momenta all $\bar{p}$'s of the beam will stop in H_2 with an improvement by a factor exceeding 10^5 compared to the $\bar{p}$ stop figure of the experiment that observed $p\bar{p}$ L X-rays in 1978[6]. These points motivate our strong support to reduce the $\bar{p}$ beam momentum as low as possible by decelerating $\bar{p}$'s in LEAR and possibly, later on, in ELENA[18]. When the momentum is below 200 MeV/c we do not gain any more in $\bar{p}$ STOP intensity, but we do gain in reduction of the stop volume. Clearly, in all cases we need a good microscopic duty cycle to record a maximum of individual $p\bar{p}$ annihilation events.

As all antiprotons of the beam annihilate in the volume surrounded by the XDC, their annihilation prongs traverse the XDC and all the chambers of the spectrometer without screening. The XDC projection chamber has a maximum drift time of the order of 2 μs. This limits the $\bar{p}$ beam intensity to $\sim 10^5$ $\bar{p}$/s for which the projection chamber images one single $\bar{p}$ annihilation event without mixing it with another one.

THE X-RAY DETECTOR

The XDC Projection Chamber

The central detector (XDC) is a projection chamber with cylindrical symmetry and radial drift electric field. It surrounds the H_2 gas target as shown in figs 8 and 10. It consists of a central cathode (with 16 cm diameter and 90 cm length) stretched between two flanges that support also field and cathode wires and field shaping disks (fig. 11). A very thin aluminized mylar foil has to be used as the central cathode of the XDC to let soft $p\bar{p}$ X-rays enter the active volume of the detector. An external rohacell tube contains the counter gas and provides the mechanical rigidity of the full structure. There are 90 resistive sense wires (R = 1500 Ω) at a diameter of 28.8 cm. 90 field wires are alternated with the sense wires and 180 external cathode wires are at 30 cm diameter. This structure provides 90 equal drift cells that point towards the axis of the detector in the absence of a magnetic field, and that take identical spiral shapes in the presence of a magnetic field parallel to the axis of the detector (see fig. 12 from ref. 10).

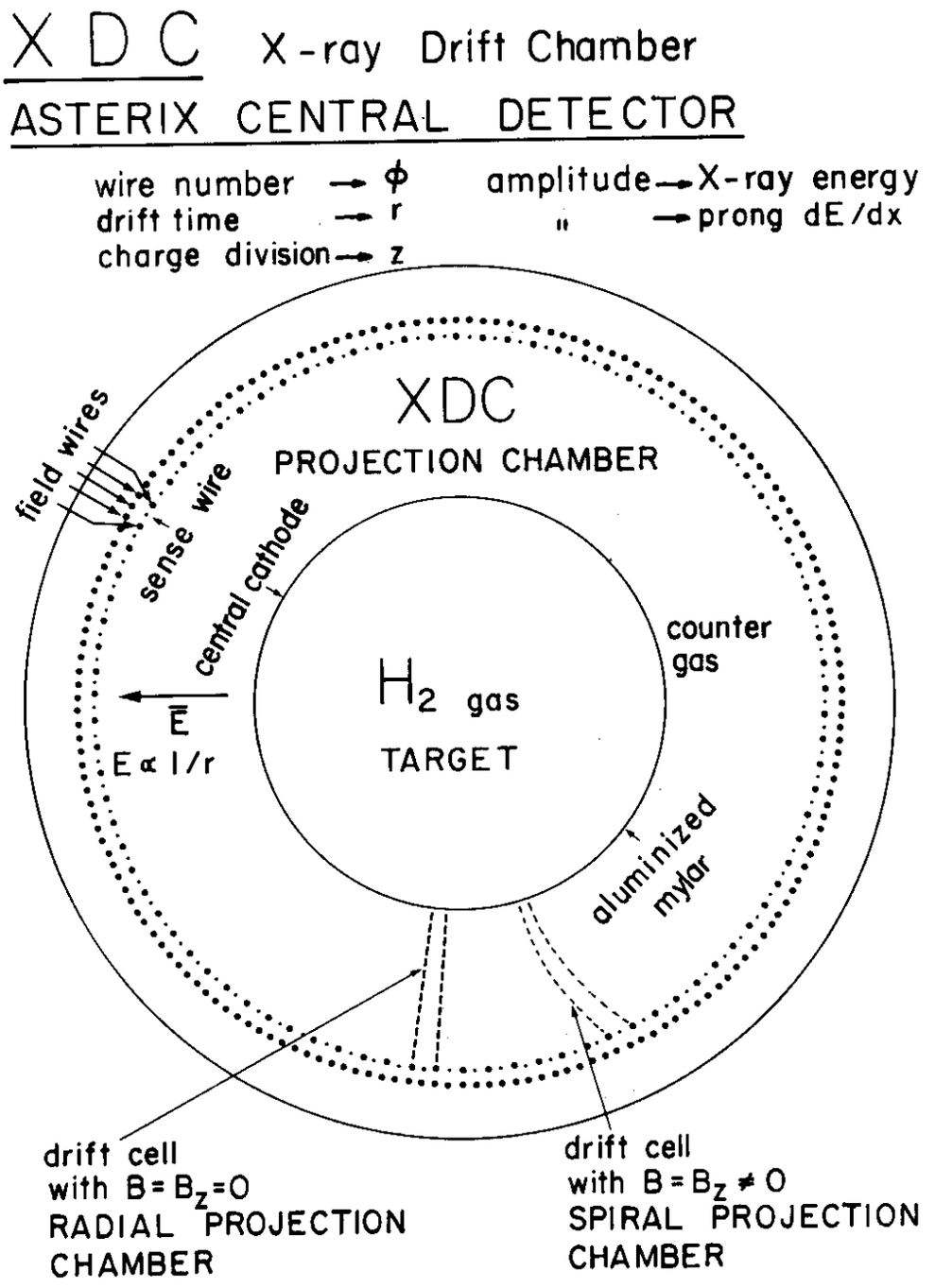

Fig. 10. Schematic view of the XDC along the target axis.

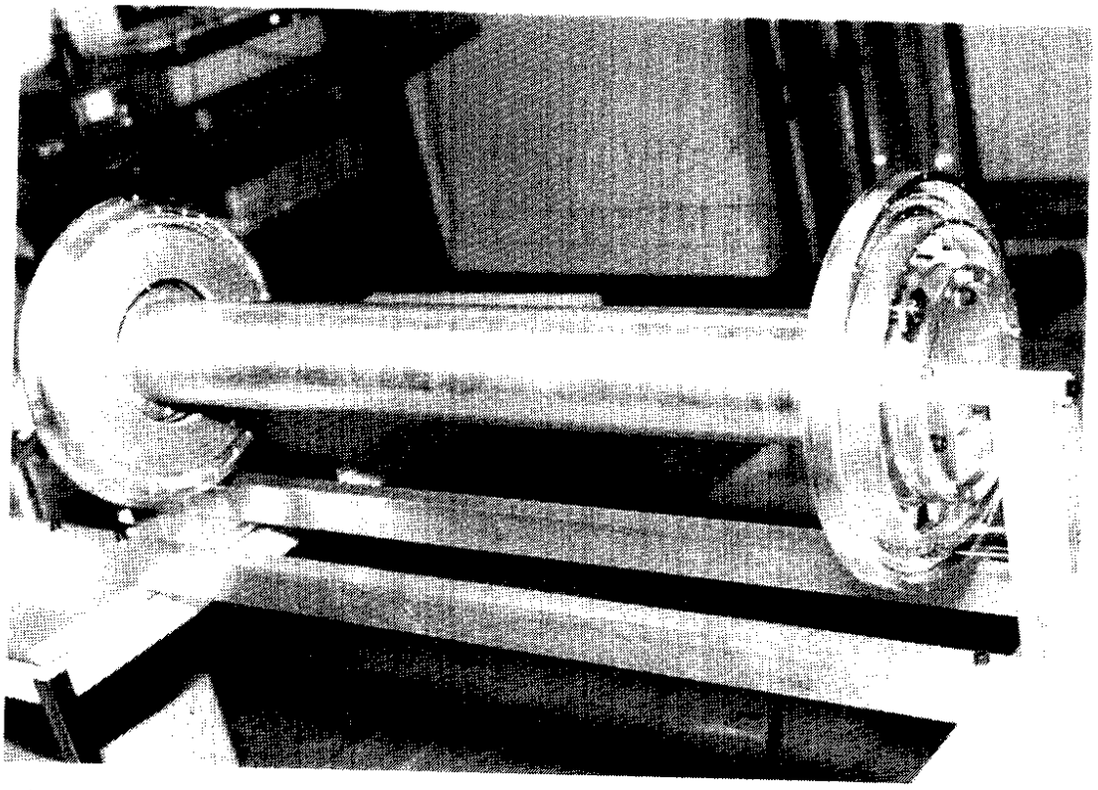

Fig. 11. XDC after completion of wiring.

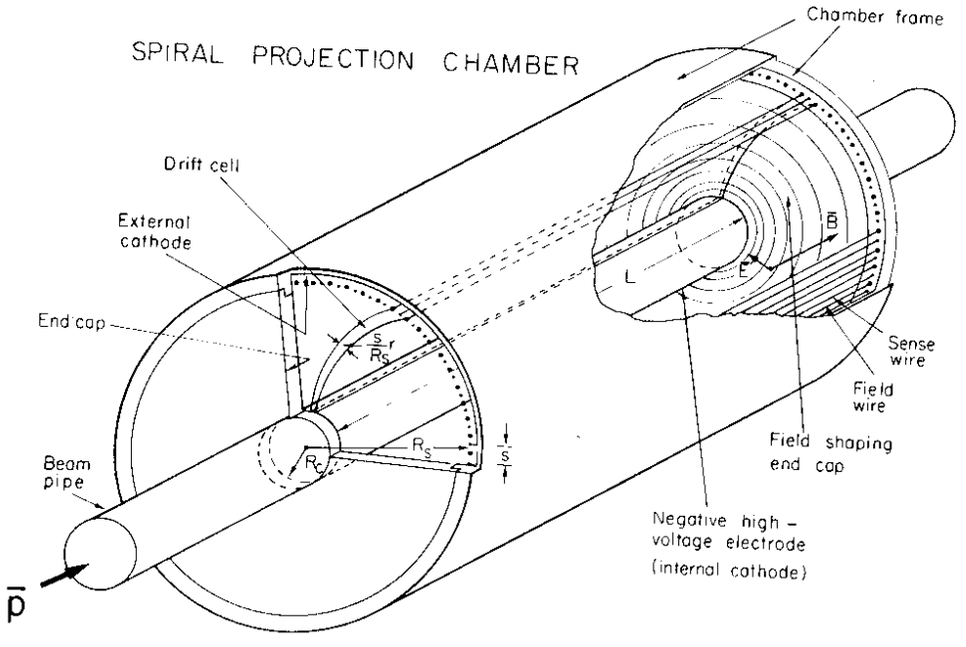

Fig. 12. Schematic structure and shape of one drift cell of a spiral projection chamber.

Electrons liberated in the counter gas by absorption of a X-ray or by the passage of an ionizing particle drift perpendicularly to the counter axis within the drift cell in which they have been produced and are multiplied near to the sense wire. Each sense wire is equipped with charge sensitive preamplifiers at its two ends. The preamplifiers are connected to CERN UA1 type read out electronics[19] that integrate and digitize the charge collected by each wire every 32 ns and keep in memory the digitized information for 4 μs. This electronics permits to localize the primary ionization in three dimensions. The wire number identifies the drift cell; the z position is obtained by charge division, and the radial position by the drift time. Moreover, the total energy deposited in each elementary volume of each drift cell is recorded. The radial thickness of each volume in a drift cell corresponds to 32 ns drift time and its extention in the z direction is determined by the resolution of the charge division method (typically ± 1 cm). The shape of the drift cells depends on the gas mixture and on the intensity of the magnetic field.

When soft X-rays are absorbed in gas the primary ionization produced around the absorption point is contained in a small volume with a size of, typically, less than 1 mm at normal pressure. Therefore an X-ray gives an isolated ionization cluster in the active volume of the XDC (see fig. 13), while a prong - e.g. from $p\bar{p}$ annihilation - will generate ions all along its track. This feature permits a clean identification of X-ray pulses.

The mean free path of X-rays in the counter gas depends strongly on the X-ray energy (fig. 14). For instance 0.6 KeV $p\bar{p}$ M X-rays travel less than 1 mm beyond the mylar cathode, and 1.7 KeV L X-rays enter typically 8 mm of the active volume. This is reflected in the drift time distributions and permits recognition of soft X-rays coming out of the target and also, by applying cuts in drift time, to trigger on soft X-rays[9]. Electronics units developed in Mainz spy into the UA1 type projection chamber data acquisition electronics and permit triggering on isolated clusters contained in a preselected drift time window, and therefore enable preferential selection of M, L or K lines. An isolated cluster on a given sense wire is defined by the requirement that the wire and the two neighbouring wires did not collect any further charge during the full drift time associated with the event.

Because of its high segmentation the XDC can detect several $\bar{p}p$ X-rays in coincidence. The detection efficiency is limited for high energy X-rays ($E \sim 10$ KeV) by the finite thickness of the counter gas, and for soft X-rays by absorption in the mylar cathode that separates the H_2 and counter gases. Fig. 15 shows the X-ray detection efficiency calculated assuming a 50/50 Ar/C_2H_6 counter gas mixture, 12 μm thick mylar window and a uniform stop distribution inside the H_2 target. In order to increase the

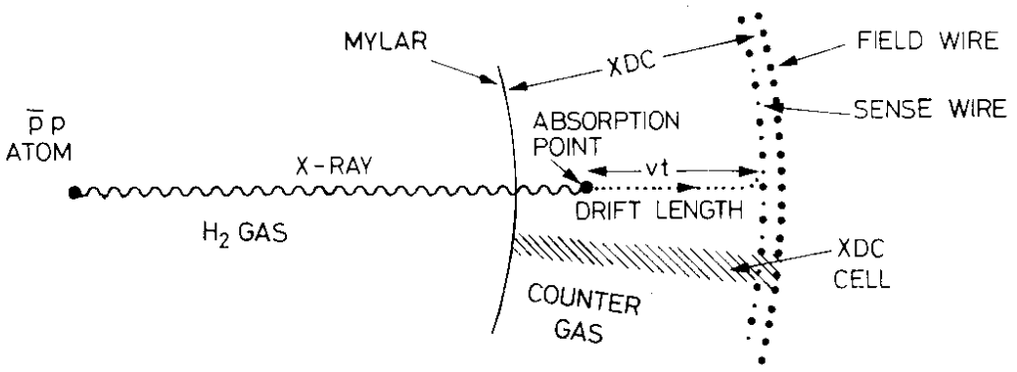

Fig. 13. Representation of an X-ray event in the XDC (B = 0).

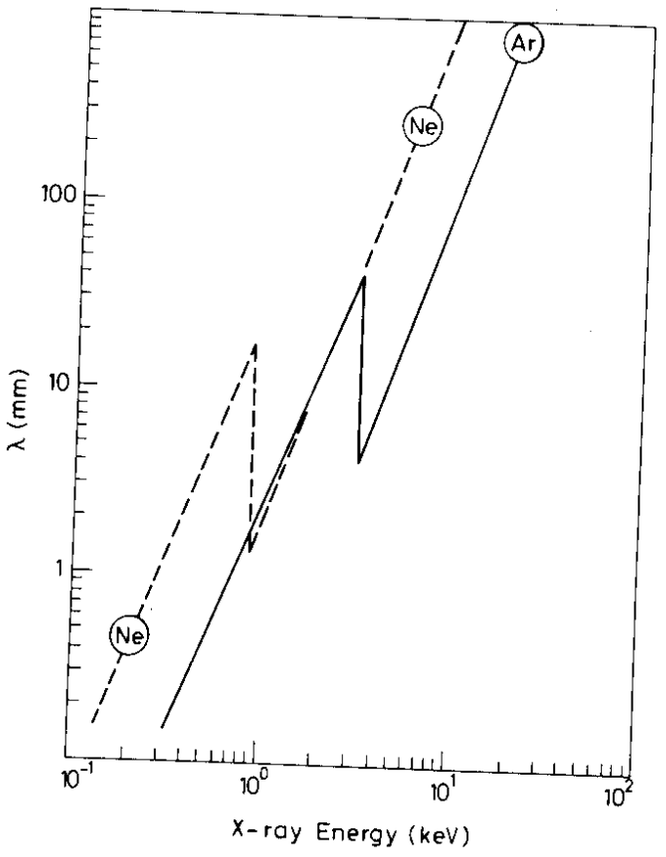

Fig. 14. Mean free path λ of soft X-rays in Ar and Ne at NTP.

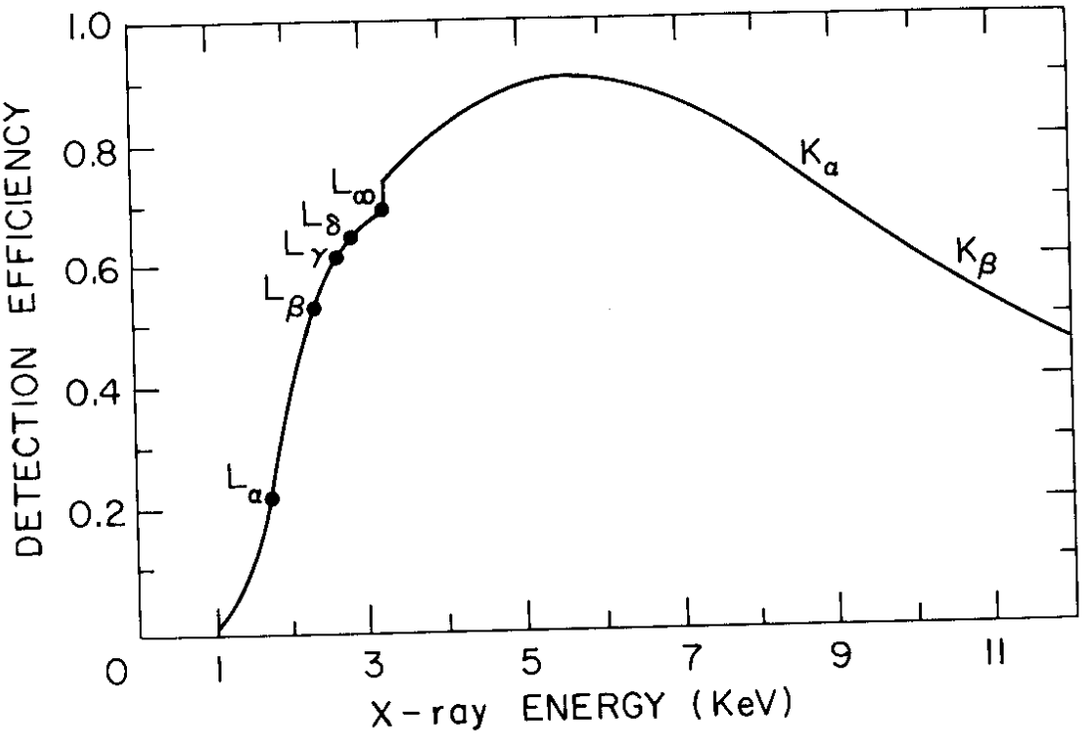

Fig. 15. X-ray detection efficiency with 12 μm mylar.

detection efficiency below 3 KeV a thinner mylar window is necessary. Operational experience exists with 6 μm windows[8], and we intend to test thinner windows too to detect $p\bar{p}$ M lines more efficiently. However, with 12 μm mylar, the typical detection efficiency for L and K X-rays is ∿ 50%.

During the data taking period of the experiment we plan to calibrate the XDC in energy, drift time and charge division with Mn^{54} and Co^{57} sources located on the scintillators T3 and T4. The γ-rays emitted in coincidence with X-rays by these sources fire the scintillators and provide calibration triggers and zero time signals.

We have constructed two XDC's which are both at present fully wired (fig 11) and one of which has been under test since January 82. One XDC is fully equipped with UA1 type electronics plus Mainz X-ray trigger electronics. The data acquisition system is operated by a PDP 11/60 computer. The results of the tests performed so far indicate that the XDC behaves qualitatively according to expectations. In the following we give a more detailed account of the XDC read-out electronics before presenting the results of some of the performed tests.

The XDC Electronics

The XDC electronics provides the following information about the pulses of the 90 sense wires:

- the total charge Q(T) as a function of time;
- the mean Z position <Z> as a function of time;
- the precise drift time after the $\bar{p}$-stop trigger;
- the pulse shape;
- the hits on neighbouring wires.

The basic principle of each sense wire readout electronics is represented in fig. 16.

The total charge Q(T) deposited on the sense wire is split into two parts Q(R) and Q(L) moving to the right or to the left end of the wire. Both ends of the wire are connected, via charge sensitive preamplifiers and twisted pair cables, to two inputs of a charge and time digitizer (CTD) module[19]. Here the sum of the two signals Q(T) = Q(L) + Q(R) and the signal from the left end of the wire Q(L) are continuously integrated over 32 ns bins.

By means of two six-bit fast analog-to-digital converters (FADC's) the digitizing electronics measures the energy loss dE/dx and the Z position every 32 ns. The dE/dx FADC digitizes the summed signal with a non-linear response function in order to increase its dynamic range. The Z position FADC uses Q(T) and Q(L) to directly give the track position along the wire. The drift time within the window of 32 ns is measured by a three-bit time-to-digital (TDC) interpolator with an accuracy of 4 ns, and an additional bit, the time tag, flags the sample at which a start of pulse (hit) has been detected.

The digital outputs of the two FADC's, the TDC and the time tag are stored in a circular 128 x 16 bit buffer memory providing a continuous record of the last 4 μs of wire information (the maximum drift time in the XDC is about 2 μs). To allow all the electronic channels to operate with identical performances and to obtain the maximum accuracy in charge division measurements, two gains and four offsets in each signal processing channel are adjustable over a small range by means of six-bit digital-to-analog converters.

Each CTD supplies the digitizing and the control electronics for 12 wires. The elementary system for the XDC data reduction is a camac crate containing one time-stop-interpolator, two CTD's, two gap-time-modules, one strobe module and one Read Out Processor (ROP). The readout electronics consists of four such crates. The ROP combines the fast handling of the CTD data with more sophisticated functions for monitoring and calibrating the XDC electronics.

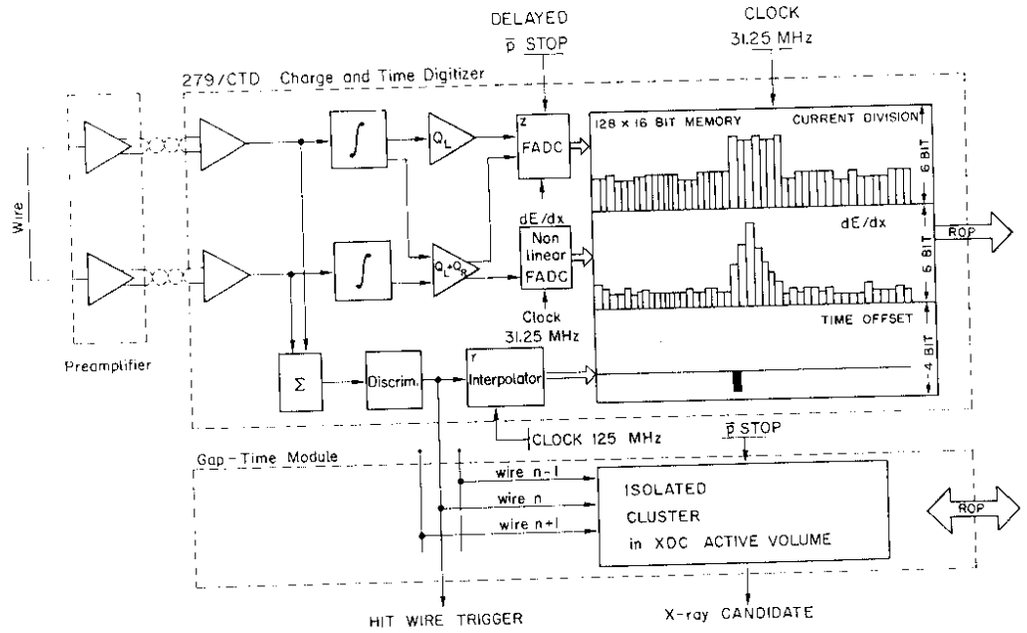

Fig. 16. Schematic block diagram of the electronics associated to each sense wire of the XDC.

The Gap Time Modules (GTM) are used for a fast discrimination of charged particles from X-rays. A GTM module provides an output for each wire with a signal if no hit has been detected on its two neighbouring wires (one gap condition). It has 12 + 2 NIM inputs derived from the time interpolator discriminator belonging to 14 adjacent wires. The two boundary signals are fed into the two neighbouring GTM's.

A strobe module generates two strobe pulses with programmable timing in order to define a drift time window for the identification of low energy X-rays with well-defined (long) drift times. The strobe pulses are used in the gap-time modules to give the one-gap-time condition.

At the occurence of a $\bar{p}$ stop trigger the CTD digitizers are stopped with a delay of 4 μs. Then, if the one-gap-time condition is fulfilled, a read signal starts the readout of the CTD buffer memories and the data formatting process under the control of the ROP processor. The results of the data reduction are stored in a 1 K fifo memory and read out by the PDP 11/60 data acquisition computer.

For each hit found, a 16 bit header word packing the wire address and the drift time is generated by the ROP followed by a variable length data block containing the CTD module number, the charge division and dE/dx samples associated with each 32 ns bin of the pulse. Information about the electronic noise is obtained by a variable number of dE/dx samples preceeding the time tag bin.

The end-of-pulse is detected by a comparison of the dE/dx samples with a given threshold. About ten 16 bit words are generated per X-ray hit and between ten and thirty for a charged particle.

After the readout of the four ROP buffer memories, the data are either written on magnetic tape or analysed on-line by the PDP. The dE/dx samples are linearized by means of a lookup table and added to give the total charge Q(T) of the pulse. The Z position <Z> is calculated as the energy weighted average over the samples taken: $\langle Z \rangle = \Sigma E_i z_i / \Sigma E_i$. Q(T), <Z>, drift time and pulse length are then stored in histograms.

During later periods of data taking, the calculation of Q(T) and <Z> will be performed by the ROP itself, reducing the output length per hit to three 16 bit words.

XDC Tests

For the purposes of the tests a 5 mm thick anticorodal tube of 16 cm diameter is used in place of the thin mylar tube and a 1 mm^2 large Mn^{54} source is positioned on the middle of this tube. A plastic scintillator mounted inside the anticorodal tube detects 835 KeV γ's from the Mn^{54} source. Several holes, closed with thin scotch tape, are positioned along 5 generatrices of the XDC container and allow externally removable X-ray sources to shine onto several sectors of the XDC's active volume. A telescope of plastic scintillators permits triggering on cosmics. The tests to be described were performed with a 50/50 Ar/CO_2 gas mixture, without powering the field shaping rings, without magnetic field, with the cathode tube set at -6 KV and the intermediate and external cathode wires set at -1.8 KV and -1.9 KV respectively; the sense wires were kept at ground potential.

Fig. 17 shows one event with an X-ray from the internal Mn^{54} source. The signals arriving at the hit wire and at the four neighbouring ones are displayed. The horizontal scale gives the drift time bin number and the vertical one gives the energy deposited in each 32 ns long drift time bin. The X-ray pulse is a short isolated one without other pulses in the same drift cell and no pulses in the neighbouring cells.

Fig. 18 shows a cosmic ray crossing several cells nearly perpendicular to the chamber axis. Each cell has a short pulse because the cosmic crosses the cell nearly normally to the drift direction. If one considered only one cell, the short isolated pulse present there could imitate a soft X-ray pulse. The total amplitude fluctuates from cell to cell according to statistics and the good time syncronization of the various cells is evident from the picture. The pulses stay on a curve, as they should do, since a straight track is seen by several wires disposed on a circle.

Fig. 19 shows a vertical cosmic ray that crosses only two XDC cells at 180°. Energy is deposited at all drift times between the maximum and the minimum. The neighbouring cells have no signal but the shape of the prong signal is very different from that of an X-ray signal. Landau fluctuations cause bin-to-bin fluctuations of the deposited energy. All kinds of situations intermediate between those displayed in figs 18 and 19 occur and in pratically all cases one can avoid accepting pulses of prongs that could imitate an X-ray pulse. These simple events also show the possibilities of using the XDC for imaging prongs that traverse it.

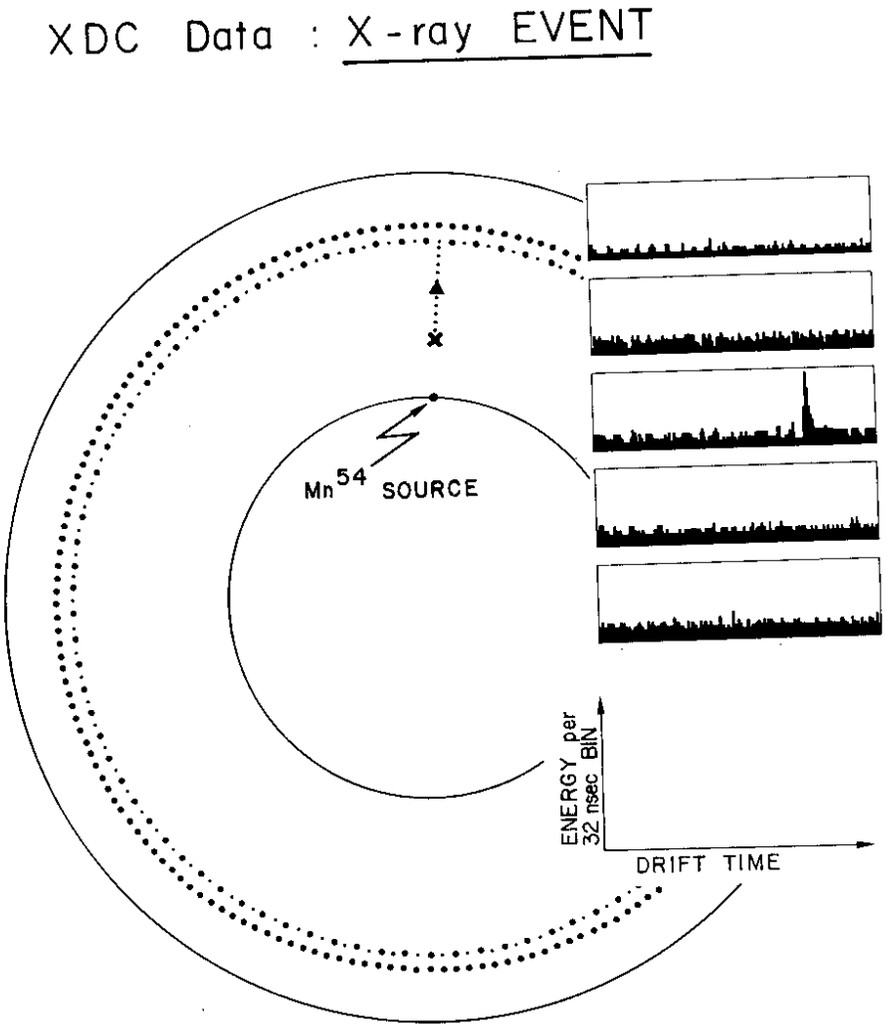

Fig. 17. X-ray event (isolated cluster in one cell, nearby cells without signal).

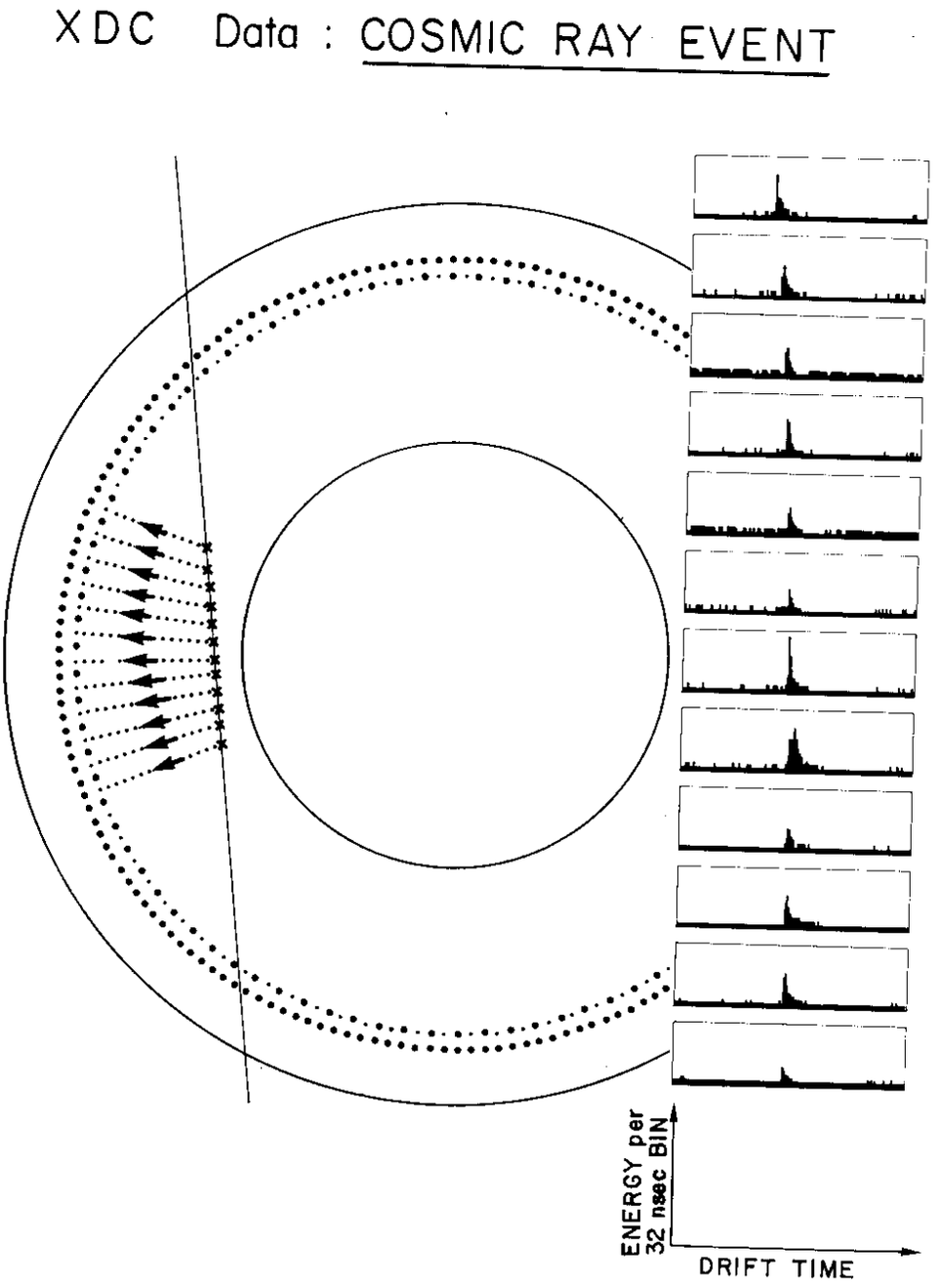

Fig. 18. Cosmic ray crossing several cells of the XDC. The track drawn in the figure is just indicative. The trigger for this event has a different delay than in figs 17 and 19.

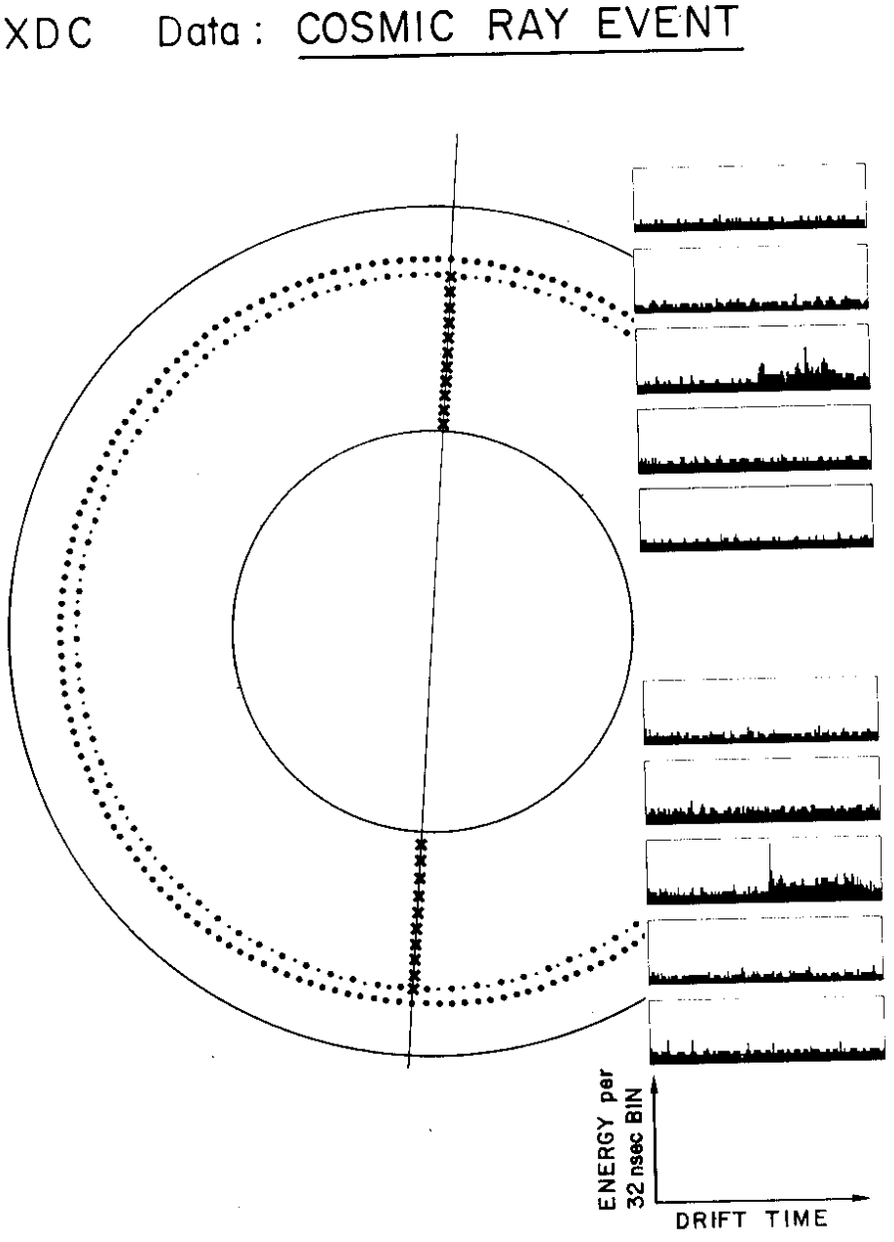

Fig. 19. Event with a cosmic ray traversing two opposite cells of the XDC.

Fig. 20 shows an energy spectrum of X-rays from a Co^{57} source positioned outside the XDC and facing one sense wire. The amplitudes of X-ray pulses of the type shown in fig. 17 are integrated over 12 drift time bins around the bin with maximum content, and the pedestal is subtracted event by event. The resulting amplitude is histogrammed in fig. 20. The horizontal scale is the X-ray energy, the vertical scale is the number of counts. One can observe in the spectrum the 3.5 KeV escape peak, the 6.5 KeV X-ray peak and, with much lower intensity, the 14.4 KeV peak. This spectrum shows that the full dynamical range of interest for protonium spectroscopy, from 1 to 15 KeV, is covered by the detector and the associated electronics.

Figs 21(a) and 21(b) show two X-ray drift time spectra from the same wire. The horizontal axis gives the drift time bin and the vertical axis the number of counts. X-ray events of the type shown in fig. 17 are included in the spectrum of (a) and (b). In fig. 21(b) there are two peaks. Data was taken with a Mn^{54} source on the internal cathode and an external Mn^{54} source. The peak on the right is due to X-rays from the internal source that are absorbed mostly in the proximity of the internal cathode and

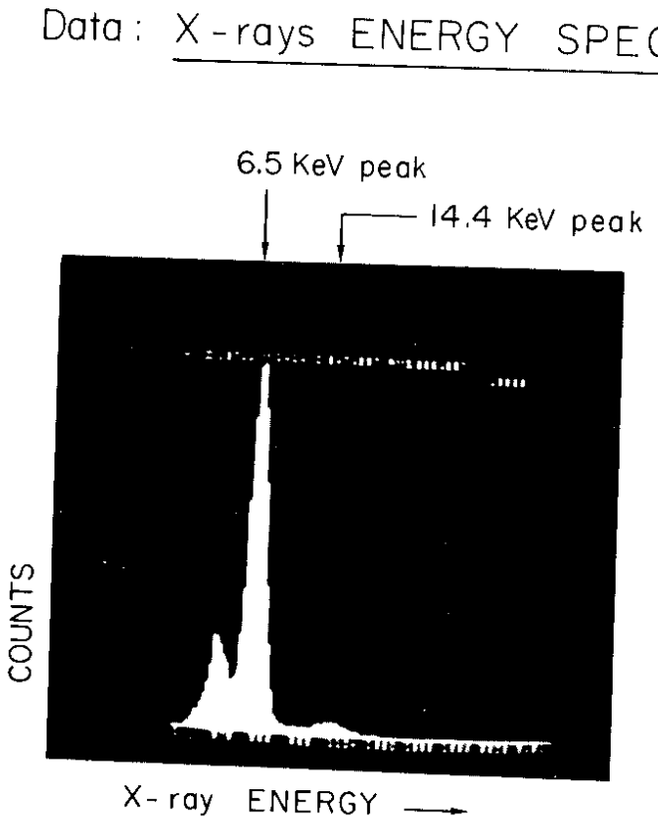

Fig. 20. X-ray energy spectrum with a Co^{57} source.

XDC Data : X-rays DRIFT TIME SPECTRA

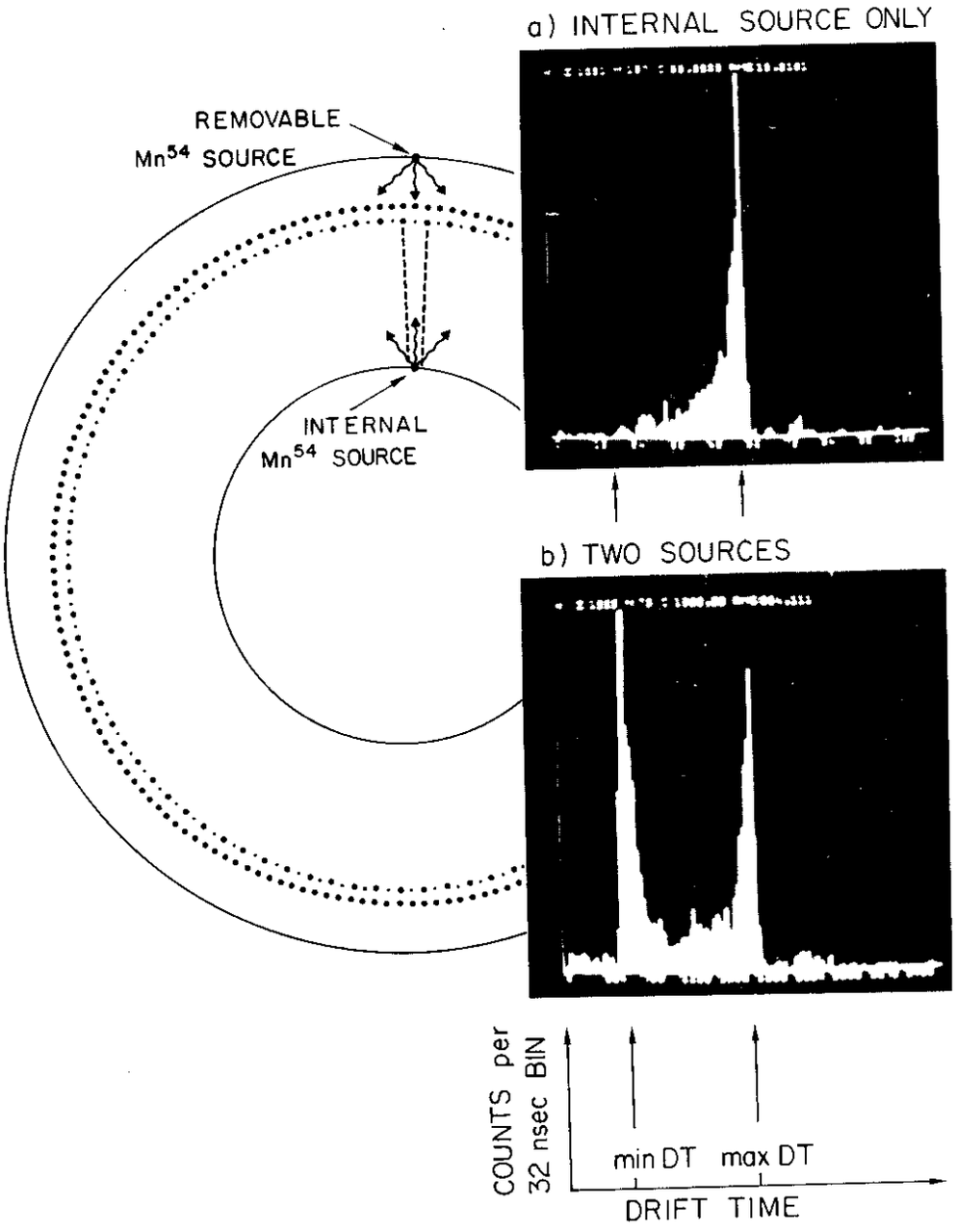

Fig. 21. Drift time spectra with X-ray sources positioned internally and externally to the XDC active volume.

whose pulses come then at maximum drift times. The peak on the left is due to X-rays from the external source that are absorbed mostly near to the sense wire, and whose pulses come then at minimum drift times. The zero time is given by plastic scintillators fired by the Mn^{54} 835 KeV γ-rays. By removing the external source one is left with the spectrum of fig. 21(a). These simple data show the power of the XDC technique: when we have a peak in the energy spectrum, then by observing the shape of the drift time spectrum of the X-rays in the peak it will be possible to distinguish an internal X-ray source from an external one.

At present, by moving the external source in z and in φ, it is found that the energy response is constant within 10%. The main work still to be done is to test the counter under operational conditions, with the mylar tube, H_2 in the target gas and the field shaping rings powered, and to map the drift lines in the magnetic field.

EXAMPLES OF ESTIMATIONS OF SIGNAL AND BACKGROUND

In order to make realistic evaluations for signals and backgrounds we start from the experimental data collected by the Protonium Collaboration[6,20,21] and make the hypothesis that, apart from a large improvement in statistics, the X-ray energy spectra will have the same characteristics, in particular the same signal to background ratios and the same resolution. This is rather pessimistic because in the conditions of the ASTERIX experiment there are the advantages introduced by the following new features:

(a) The $\bar{p}$ annihilation vertex is reconstructed for each event and is required to be inside the H_2 target.

(b) The $\bar{p}$ beam is not contaminated and most of the $\bar{p}$'s stop inside the H_2 target (in the Protonium experiment less than 0.1% of the incoming antiprotons were stopping in H_2).

(c) By working at 1 atm instead of 4 atm the absolute yield of $\bar{p}p$ X-rays increases because of reduced Stark mixing.

(d) The X-ray identification is substantially improved (pratically no prong should be able to imitate an X-ray signal).

(e) It is possible to establish whether the source of an X-ray line is internal or external to the H_2 target.

(f) To reduce the noise below the L-line signal it will be possible, when working with a mylar window thinner than 6 μm, to require an M X-ray in coincidence with each L X-ray.

In order to work out some simple numerical estimates to get the order of magnitude of the effects, we make the following simplifications and assumptions:

Detection efficiency for L X-rays:	$E_L = 50\%$
Detection efficiency for K_α X-rays:	$E_K = 50\%$
Yield of L X-rays at 1 atm: (pessimistic as this is already the 4 atm yield).	$Y_L = 5\%$
Yield of K_α X-rays: (under the assumption that the 2P level annihilates in 99% of the cases).	$Y_{K_\alpha} = 0.05\%$
Yield of background X-rays per event in a 2 KeV wide energy region centered at 2 and at 8 KeV.	$Y_B \simeq 1\%$

Protonium Spectroscopy

We consider a run with 10^7 $\bar{p}$ stopped in H_2. In a 2 KeV wide window centered on a $\bar{p}p$ X-ray line we expect then the following:

L X-rays:	
Signal = $10^7 \times Y_L \times E_L$	= 250 000
Background = $10^7 \times Y_B$	= 100 000
Significance of effect = $\frac{S}{\sqrt{S+B}}$	≃ 400
K_α X-rays in singles:	
Signal = $10^7 \times Y_K \times E_K$	= 2 500
Background K_α = $10^7 \times Y_B$	= 100 000
Significance of effect	≃ 8
K_α X-rays in coincidence with L X-rays:	
Signal = $10^7 \times Y_L \times E_L \times (\Gamma^{RAD}/\Gamma^{ANN})_{2P} \times E_K$	= 1 250
Background = $350\,000 \times Y_B$	= 3 500
Significance of effect	≃ 18

In the protonium experiment[6] the total number of $\bar{p}$'s stopped in H_2 gas at 4 atm was 150 000 and this required about two weeks of data taking. In the ASTERIX experiment we will be limited by the speed at which events can be written on tape. Due to the

complexity of the information to be written it will be possible to put on tape about 100 events per second.

From table 1 one sees that we can always have 100 $\bar{p}$ stops/s at all beam momenta below 600 MeV/c with less than 10^4 $\bar{p}$/s beam intensity. Therefore, we should be able in 10^5 s of data taking with the minimum biased $\bar{p}$ stop trigger to find the K_α line with more than 1000 events and to measure the annihilation width of the 2P level with a 10% accuracy.

Search of K_α Transitions to the Triplet Ground State

A $\pi^+\pi^-$ final state in coincidence with a K_α X-ray implies that the K_α X-ray populated a triplet ground state. The branching ratio of the channel $\pi^+\pi^-$ is 4 10^{-3}, and its overall detection efficiency is $\simeq$ 50%. To establish the $^3S_1$ line with 1000 (K_α, L) coincidences about $10^3/(10^{-4} \cdot 2\ 10^{-3}) = 5\ 10^9$ events corresponding to 5.10^7 seconds of data taking would then be necessary with the simple $\bar{p}$ stop trigger. We envisage, however, to trigger the data acquisition by requiring on line in the trigger a $\pi^+\pi^-$ final state (collinear $\pi^+\pi^-$) and/or an X-ray in the K_α energy region. Then the data acquisition would not be saturated even if both triggers are selective only at the 1% level. At 300 MeV/c beam momentum one could have:

6 10^4 $\bar{p}$/s beam.

10^4 $\bar{p}$ stop triggers/s

20 events with $\pi^+\pi^-$/s.

2.4×10^{-3} events with a ($\pi^+\pi^-$, K_α, L) coincidence/s.

To get 1000 K_α X-rays of the $^3S_1$ line, 4 10^5 s of data taking would then be necessary.

Search of Resonances in P-wave Annihilations

6 10^4 $\bar{p}$/s beam.

10^4 $\bar{p}$ stop triggers/s.

250 events with L X-ray/s.

With a selective L X-ray trigger we could then collect up to 100 $\bar{p}p$ annihilations from the 2P level per second and, in order to get a sample of 10^8 P-wawe annihilation events, about 10^6 s of data taking would be necessary.

Search of Resonances in S-wave Annihilations

$6\ 10^4\ \bar{p}$/s beam.

$10^4\ \bar{p}$ stop triggers/s.

1.2 (L, K) events/s.

It could be worthwhile collecting a large data sample of events with detected K_α X-rays if the singlet and triplet ground states are separated as shown in fig. 6 and the XDC can distinguish between the two lines.

To compare singlet and triplet S-wave annihilations with a data sample of 10^7 events, about 10^7 s of data taking would be necessary! This data taking time could be reduced by a factor of 10 with a beam momentum below 200 MeV/c, for which all $\bar{p}$ would stop in the H_2 target. In order not to saturate the data acquisition system the (L, K_α) trigger should have a selectivity better than 10%.

ACKNOWLEDGEMENTS

The Mainz group of the collaboration is responsible for the central detector of the ASTERIX experiment. For the development and construction of the XDC and of its electronics substantial assistance was provided by the CERN EP groups of G. Muratori and H. Verweij. We also should like to thank the CERN EF group of P. Queru and the technical support groups in Orsay and München for their assistance. Discussions with colleagues working with the central detectors of the UA1 and AFS spectrometers were very helpful during the design phase. The work of the Mainz and München groups is partially supported by the Bundesministerium für Forschung und Technologie, Bonn, Federal Republic of Germany.

REFERENCES

1. R. Armenteros, E.G. Auld, D.A. Axen, G.A. Beer, J.C. Bizot, L. Cerrito, M. Comyn, W. Dahme, B. Delcourt, K.L. Erdman, P. Eschstruth, U. Gastaldi, G. Gräff, R. Howard, J. Jeanjean, H. Kalinowsky, F. Kayser, E. Klempt, R. Landua, C.J. Martoff, L.P. Robertson, Ch. Sabev, R. Schneider, O. Schreiber, U. Straumann, P. Truöl, J.B. Warren, B.L. White and R.W. Wodrich, A study of $p\bar{p}$ interactions at rest in a H_2 gas target at LEAR, CERN/PSCC 80-101 (1980).
2. For a review of work previous to 1969, see R. Armenteros and B. French, NN interactions, in High Energy Physics (ed. E.H.S. Burhop) (Academic Press Inc., New York, 1969), vol. 4, p. 383. Ref. 1 gives in sect. 2 an updated overview restricted to $p\bar{p}$ interactions at rest.

3. J. Jeanjean, M. Jeanjean, R. Madaras, J.L. Masnou, J. Perez-Y Jorba, A. Quenzer, F. Rumpf, J.L. Bertrand, J.C. Bizot, R.L. Chase, A. Cordier, B. Delcourt, P. Eschstruth and G. Grosdidier, Nucl. Instr. and Meth. 117 (1974) 349;
A. Cordier, B. Delcourt, P. Eschstruth, F. Fulda, G. Grosdidier, J. Haissinski, J. Jeanjean, M. Jeanjean, R. Madaras, J.L. Masnou, J. Perez-Y Jorba, A. Quenzer, F. Rumpf, J.L. Bertrand, J.C. Bizot and R.L. Chase, Nucl. Instr. and Meth. 133 (1976) 237.
4. ASTERIX Collaboration, qq spectroscopy and search for glueballs, baryonia and other boson resonances in $p\bar{p}$ annihilations at rest with the ASTERIX experiment at LEAR, report to this workshop.
5. For a review see J.M. Richard, Protonium and other exotic $\bar{p}$ atoms, report to this workshop.
6. E.G. Auld, H. Averdung, J.M. Bailey, G.A. Beer, B. Dreher, H. Drumm, K. Erdman, U. Gastaldi, E. Klempt, K. Merle, K. Neubecker, C. Sabev, H. Schwenk, V.H. Walther, R.D. Wendling, B.L. White and W.R. Wodrich, Phys. Lett. 77B (1978) 454.
7. U. Gastaldi, E. Iacopini and R. Landua, Atomic cascades in vacuum of pp atoms formed in flight with the reaction $p + H \rightarrow p\bar{p} + 2\ e^-$, CERN p LEAR Note 21, 1979.
8. U. Gastaldi, R.D. Wendling, E.G. Auld, H. Averdung, J. Bailey, G.A. Beer, B. Dreher, K.L. Erdman, E. Klempt, K. Merle, K. Neubecker, C. Sabev, H. Schwenk, B.L. White and R. Wodrich, Nucl. Instr. and Meth. 156 (1978) 257.
9. U. Gastaldi, Nucl. Instr. and Meth. 157 (1978) 441.
10. U. Gastaldi, Nucl. Instr. and Meth. 188 (1981) 459.
11. For a review see R. Bizzarri, Nuclear-antinucleon annihilation at low energies, report to this workshop.
12. See e.g. R. Landua, The atomic cascade in pp and implications for pp annihilations at rest, report to this workshop and refs. therein.
13. C.B. Dover, J.M. Richard and M.C. Zabek, Ann. of Phys. 130 (1980) 70.
14. For a review see T. Barnes, Meson resonances and glueballs: theoretical review and relevance to $p\bar{p}$ at LEAR, report to this workshop.
15. For a review see, D. Scharre, Glueballs - a status report, SLAC Report SLAC-PUB 2880 (1982).
16. R. Armenteros, D.N. Edwards, T. Jacobsen, A. Shapira, J. Vandermeulen, C. d'Andlau, A. Astier, P. Baillon, H. Briand, J. Cohen-Ganouna, C. Defoix, J. Siaud, C. Ghesquière and P. Rivet, Proc. Intern. Conf. Elementary Particles, Sienna, 1963, 1, 287, Soc. Ital. di Fis., Bologna.
17. P. Baillon, D. Edwards, B. Maréchal, L. Montanet, M. Tomas, C. d'Andlau, A. Astier, J. Cohen-Ganouna, M. Della Negra,

S. Wojicicki, M. Baubillier, J. Duboc, F. James and F.R.Lévy, Nuovo Cimento, 50 (1967) 393.

18. H. Herr, A decelerator ring for Extra Low ENergy Antiprotons (ELENA), report to this workshop.
19. M. Calvetti, S. Cittolin, C. Cochet, C. Engster, B. Hallgren, H. Hoffman, V. Karimaki, L. van Koningsveld, J.P. Laugier, B. Lovstedt, G. Maurin, A. Norton, P. Petit, G. Piano Mortari, A. Placci, P. Queru, M. Rijssenbeek, C. Rubbia, B. Sadoulet, W. Scott, K. Sumorok, C. Tao and H. Verweij, Nucl. Instr. and Meth. 176 (1980) 255.
20. E.G. Auld, J.M. Bailey, G.A. Beer, B. Dreher, H. Drumm, K. Erdman, U. Gastaldi, H. Kalinowsky, E. Klempt, K. Merle, K. Neubecker, C. Sabev, R.D. Wendling, B.L. White and W.R. Wodrich, Proc. 4th European Antiproton Symposium, Barr-Strasbourg, 1978 (ed. A. Friedman) (Editions du CNRS, Paris, 1979), Vol. 1, p. 115.
21. R.W. Wodrich, E.G. Auld, J.M. Bailey, G.A. Beer, B. Dreher, U. Gastaldi, H. Kalinowsky, E. Klempt, R. Landua, K. Merle, K. Neubecker, Chr. Sabev, R.D. Wendling and B.L. White, Nucl. Phys. A334 (1982) 386.